Published in final edited form as:

IEEE Trans Med Imaging. 2019 June ; 38(6): 1427–1437. doi:10.1109/TMI.2019.2895779.

Monitoring acute stroke progression: multi-parametric OCT imaging of cortical perfusion, flow, and tissue scattering in a mouse model of permanent focal ischemia

Woo June Choi,

School of Electrical and Electronics Engineering, College of ICT Engineering, Chung-Ang University, Seoul, 06974, Korea

Yuandong Li,

Department of Bioengineering, University of Washington, Seattle WA 98195, USA

Ruikang K. Wang*

Department of Bioengineering and Department of Ophthalmology, University of Washington, Seattle WA 98195, USA

Abstract

Cerebral ischemic stroke causes injury to brain tissue characterized by a complex cascade of neuronal and vascular events. Imaging during early stages of its development allows prediction of tissue infarction and penumbra, so that optimal intervention can be determined in order to salvage brain function impairment. Therefore, there is a critical need for novel imaging techniques that can characterize brain injury in the earliest phases of ischemic stroke. This study examined optical coherence tomography (OCT) for imaging acute injury in experimental ischemic stroke in vivo. Based on endogenous optical scattering signals provided by OCT imaging, we have developed a single, integrated imaging platform enabling the measurement of changes in blood perfusion, blood flow, erythrocyte velocity, and light attenuation within cortical tissue, during focal cerebral ischemia in a mouse model. During the acute phase (from 5 minutes to the first few hours following blood occlusion), the multi-parametric OCT imaging revealed multiple hemodynamic and tissue scattering responses in vivo, including cerebral blood flow deficits, capillary non-perfusion, displacement of penetrating vessels, and increased light attenuation in the cortical tissue at risk that are spatially correlated with the infarct core, as determined by postmortem staining with triphenyltetrazolium chloride (TTC). The use of multi-parametric OCT imaging may aid in the comprehensive evaluation of ischemic lesions during the early stages of stroke, thereby providing essential knowledge for guiding treatment decisions.

*Corresponding author, phone: 206-616-5025; fax: 206-616-5025; wangrk@uw.edu.

Conflicts of interest

Dr. Wang discloses intellectual property owned by the Oregon Health and Science University and the University of Washington related to OCT angiography, and licensed to commercial entities, which are related to the technology and analysis methods described in parts of this manuscript. All other co-authors declare no disclosures.

Index Terms—

acute ischemic stroke; multi-parametric optical coherence tomography; hemodynamic and tissue scattering responses

I. Introduction

In ischemic stroke, the evolution of brain injury following an occlusive event spans a temporal continuum of presentation, from hyperacute (minutes), to acute (hours), and ultimately, to chronic (days) phases. Within minutes of an occlusion event, brain tissue at the center of the ischemic insult experiences the most drastic reduction of blood volume, reaching 10 ml/100g/min (20 % of normal) and below, creating a severe hypoxic environment that results in necrosis of neurons [1]. Such necrotic tissue, also characterized as an infarct core, is surrounded by a peripheral zone, a rim of hypoperfused (10–20 ml/100g/min; about 30–40 % of normal) tissue referred to as the ischemic penumbra [1][2]. Unlike the infarct core, the penumbral zone is functionally suppressed, yet remains structurally and metabolically intact. Timely reperfusion to the penumbra provides an opportunity for the functional recovery of the salvageable tissue before it permanently develops into infarction within hours. Therefore, understanding and delineating the hemodynamic events occurring at the salvageable brain tissue is critically important for designing targeted treatment during the acute phases of stroke [3] [4].

Cerebral imaging after stroke onset prior to therapeutic intervention provides invaluable information regarding the severity and extent of brain tissue ischemia under development, which is crucial for determining timely treatment protocols and evaluating the prognosis of therapies. Several important cerebral perfusion imaging techniques have been used in previous stroke studies in animals and humans, including positron emission tomography (PET) [5], diffusion/perfusion-weighted magnetic resonance imaging (MRI) [6], and perfusion computed tomography (PCT) [7]. PET has been considered the current standard of care for *in vivo* detection of infract core and penumbra, through an assessment of the relationship between the combined imaging of the regional cerebral blood flow (CBF) and brain metabolism. However, its availability is restricted by the complex logistics involved in its use, and exposure of the brain to radiation is inevitable because of the use of radioactive tracers for detecting changes in vascular transit times caused by circulatory disturbances [8]. Moreover, the required delay between tracer injection and imaging is too long (greater than 2 hours), which further limits the broad application of PET for therapeutic decision-making in acute ischemic stroke [9]. Diffusion/perfusion-weighted MRI is widely available and has become the routine method for acute evaluation of stroke, where the area of diffusion/perfusion mismatch has been used as a surrogate marker for the penumbra in early stroke patients [6] [10] [11]. Despite promising clinical outcomes, there has been a fundamental controversy regarding the definition of the ischemic-compromised tissues using such diffusion/perfusion mismatch approaches, due to methodological limitations [12][13], PCT has been applied to conventional fast CT scanners for cerebral perfusion imaging, which has shown useful for rapid assessments of the early ischemic penumbra and infarct core. Similar

to PET, however, this method requires the administration of invasive radioactive contrast medium, imposing a radiation burden on the body.

Recently, functional optical coherence tomography (OCT) has emerged as a potential candidate for monitoring acute ischemic strokes in preclinical investigations. OCT is a non-invasive, label-free optical imaging technique capable of resolving microanatomy of living biological tissues over a field-of-view of several millimeters, with micron scale resolution [14]. Recent developments in OCT scan protocols and post-processing algorithms have enabled the derivation of functional OCTs that can gather information regarding blood perfusion [15] and blood flow velocity [16], as well as optical properties [17] of perfused tissues. Notably, studies have used OCT angiography (OCTA) to explore cortical vasculature and hemodynamics in ischemic stroke models of mice *in vivo* [18]–[24]. OCTA enhances the motion-contrast of red blood cells (RBCs) moving through the vessel lumen, permitting visualization of fine vascular networks and circulation in the mouse cerebral cortex without the need for exogenous contrast agents [21]. For an accurate determination of the extent of ischemic injury, moreover, a tissue characterization technique using OCT signals is proposed. This method creates a map of optical attenuation coefficients for cortical tissues across the mouse cortex, in which the attenuation coefficients are measured by analyzing the decay of the received OCT signals due to light absorption and scattering [17][23][24]. Changes in the attenuation in the injured cortical tissue may be used to differentiate the ischemic core from penumbra [17][23][24]. In all previous studies using OCT, monitoring of ischemic injury has been typically examined in the mouse brain a few hours after stroke onset. Although this approach was adequate in assessing hemodynamic and tissue property change as a result of the ischemic injury, key pathophysiologic events occurring within minutes to hours after the blood vessel occlusion remain unknown. To our best knowledge, such events that may be critical to rescue penumbra were not documented in the prior literature.

In this report, we monitor hemodynamic and structural changes in the mouse brain minutes after stroke onset to the first 3 hours using a single OCT imaging platform. A distal middle cerebral artery occlusion (dMCAO) model is used to induce focal ischemic stroke in the mouse brain. The OCT imaging platform provides multiple measures of blood perfusion, velocity, flow, and light attenuation, from which the evolving changes in cortical vasculature, CBF, capillary perfusion, and tissue scattering during the acute phases of stroke are characterized. This comprehensive assessment of vascular and tissue injury revealed distinct events occurring at ischemic penumbra and infarct cores.

II. Experimental procedures and animal PREPARATION

All experiments performed on animals were terminal and the protocols were reviewed and approved by the Institutional Animal Care and Use Committee of the University of Washington, Seattle. Male, 8-week-old, C57BL/6J mice (n=5), weighing 20–25 g (Charles River Laboratories, Hollister, CA), were used in this study. Prior to the experiments, animals were housed at room temperature (22 °C), in a 12-hour light dark cycle, and provided access to pelleted food and water *ad libitum*.

A. Open-skull cranial window preparation

Open-skull cranial window surgery was performed on the right parietal bone [25]. In preparation for the surgery, the mouse was initially anesthetized with isoflurane inhalation in 0.2 L/min O_2 and 0.8 L/min air and subsequently maintained with a sufficient level of anesthesia throughout the experiment. Body temperature was maintained between 36.8–37 °C with a homeothermic heating pad (50–7220F, Harvard Apparatus, Cambridge, MA, USA) controlled by a rectal thermometer. Following induction of anesthesia, the animal was placed on a stereotaxic frame in a prone position and its head was stabilized with ear bars. Lubricant ointment was applied to the eyes to prevent drying. A 4 mm by 4 mm craniotomy was performed 1 mm posterior and lateral to bregma, using a dental drill (Foredom Electric Co., Ethel, CT, USA). A circular piece of skull was carefully detached using fine forceps and replaced with a round, transparent glass coverslip measuring 5 mm in diameter. Cyanoacrylate cement was used to seal the glass coverslip to the skull, yielding a 3 mm by 3 mm flat tissue surface as an imaging window, through which major pial vessels in the somatosensory cortical region were visible under the microscope. After baseline imaging of the mouse was completed, the dMCAO procedure was performed.

B. Permanent dMCAO model

To induce focal is chemic stroke in the mice, direct coagulation of the distal middle cerebral artery (MCA) was performed [26], Following baseline imaging, the anesthetized mouse was placed in a lateral position on the surgery table, and a 1 cm incision was made in the skin between the lateral part of the orbit and the external auditory canal. The skin was retracted using hook retractors and the temporal muscle underlying the skin was partially dissected and pushed aside to expose the skull. After resecting the muscle, the cortical arteries were viewed through the partially translucent mouse skull. A 1 mm burr hole was drilled on the exposed frontal bone, while being cautious not to apply downward pressure. When the bone became thin enough to see the underlying MCA branch, it was carefully withdrawn with thin forceps. Then, the proximal and distal sides of the MCA bifurcation were coagulated, by gently touching the artery with bipolar cauterizing forceps, until fully occluded. After the temporal muscle and skin were relocated to their positions, the animal was returned to the prone position and quickly transferred to the imaging table for OCT imaging. The post-surgical process, including transfer to the imaging table and positioning prior to the OCT imaging, took 5–8 minutes after the MCA occlusion was completed.

C. TriphenyltetrazoHum chloride staining

To locate the infarct, we used 2,3,5-triphenyltetrazolium chloride (TTC) staining, a standard method for fast and reliable delineation of cerebral ischemic injury. When the imaging was completed (3 hours after ischemia), the mice were euthanized and perfused transcardially with 0.1 M phosphate buffered saline (PBS, pH 7.4). Then, the brain was isolated and sliced rostro-caudally into serial 2 mm thick slices, using a mouse brain slicer. The slices were incubated in 2 % TTC, in saline, for 30 minutes at 37 °C, after which the stained slices were reassembled along the rostral-caudal axis. Images of TTC-stained brain sections were obtained using a digital camera.

III. Imaging and data analysis

A. Imaging platform description

We used a custom-designed, 1300 nm spectral domain OCT (SD-OCT) system for *in vivo* imaging of the mouse cerebral cortex. The system specifications were described previously [27]. In brief, the light source consisted of a matched pair of superluminescent diodes (SLD) having offset emission spectra, yielding a combined light spectrum with a central wavelength of 1340 nm, and a bandwidth of 110 nm at 3 dB, giving a measured axial (depth) resolution of ~7 μm in air. A 2 × 2 fiber coupler divided the light into two paths with a ratio of 10:90 for optical power, for the reference arm and sample arm, respectively. Light reflected from the sample interfered with the reference light, which was then spectrally detected by a custom spectrometer consisting of a transmission grating, an achromatic double lens, and a 1024-pixel InGaAs line scan camera operated at 92,000 axial scans per second. A 10 × objective lens was used to deliver the probing light into the sample, yielding a lateral resolution of ~7 μm in air. The system sensitivity was measured at ~104 dB with a 3.5 mW light on the sample. To enable imaging, a pair of x-y galvanometric scanners was employed to steer the probe beam along the transverse (x-axis) and elevational (y-axis) directions, providing cross-sectional (2-D) as well as three-dimensional (3-D) OCT datasets.

B. OCT Angiography

The OCT signal received from the tissue sample is a result of linear superposition of static, dynamic scattering components and additive system noise, in which the dynamic scattering component can be assumed to be due mainly to moving RBC scatters. OCTA works to extract the moving scattering elements of the OCT signal in order to localize blood perfusion within the scanned tissue. In this study, we employed a simple and highly sensitive OCTA approach, optical microangiography (OMAG), that measures differentiation in the time-scale of complex OCT signals [28][29]. The algorithm computes inter-frame differences in the acquired 3-D OCT dataset, yielding power of the dynamic scattering components proportional to the scattering from RBCs. The OCTA scan protocol acquired 8 repeated B-scans at each transverse y location, and each B-scan consisted of 400 A-lines along the x location (fast axis). At the completion of scanning, a total of 3200 B-scans were captured at 400 y locations (slow axis) over a cortical surface area of 4 mm by 4 mm. To process the data, differential operations between the adjacent frames of the repeated ensemble B-scans were performed, and the absolute values were averaged along the transverse y location. Finally, the processed OCTA cubic data was collapsed into two-dimensional data with a maximum amplitude projection (MAP), where the highest amplitude along the depth was chosen for each A-line, creating an *en face(x-y)* vascular map involving the perfused microvessel network. Figs. 1A and 1B show representative cross-sectional (x-z) OCT and OCTA images of a healthy adult mouse brain with a coverslip over the cranial window, exhibiting the structure and blood perfusion in the neocortex. In Figs. 1G and 1H, structural and vascular maps, respectively, generated from the 3-D OCT and OCTA datasets, segmented from the surface to a depth of 350 μm (between the two red dotted lines in Fig. 1A), are shown. The vascular map delineates pial vasculatures, diving arterioles and ascending venules as well as complex capillary beds throughout the laminar cortical layers 1

and 2/3 [30]. The periodic bright lines appearing along the MCA (arrow) in Fig. 1H are due to pulsatility-induced motion artifacts.

C. Flow velocity

Blood flow velocity was calculated using Doppler optical microangiography (DOMAG), a technical extension of Doppler OCT (DOCT), in which DOCT is combined with the OMAG technique [31]. Analogous to DOCT, DOMAG deduces the axial (z) projection component of flow velocity:

$$V_z = \lambda_0 \Delta\phi/(4\pi nT), \quad (1)$$

where λ_0 is the central wavelength of the light source, n is the tissue refractive index, and $\Delta\phi$ and T are the phase difference (involving a Doppler frequency shift) and the time interval between adjacent A-scans, respectively. The main difference between DOMAG and DOCT is the use of a high-pass filter in OMAG prior to the Doppler algorithm; a differential operation of the complex OCT signals between inter A-scans is taken to eliminate the static scattering signals:

$$d(i) = c(i+1) - c(i), \quad (2)$$

where i is the index of the A-scan number and $c(i)$ is the complex signal of the I-th A-scan. Accordingly, the high pass filtering allows for enhancement of the flow sensitivity [28], Then, the Kasai autocorrelation method was used to obtain the phase difference:

$$\Delta\phi = \angle\left\{\sum i[d(i+1)d^*(i)]\right\}, \quad (3)$$

where * and $\angle$ denote the symbols of complex conjugate and angle, respectively. For the DOMAG scan protocol, the fast axis (x) scanner was driven by a step waveform with 300 steps for one B-scan. In each step, 25 A-scans were repeatedly acquired (M-mode scan), thus the total number of A-scans in each B-scan was 7,500. In the slow axis (y) direction, 300 B-scans were captured over the 4 mm by 4 mm cortical surface. Blood flow velocities in individual vessels were deduced from the acquired 3-D complex OCT dataset using the DOMAG algorithm mentioned above, and the resulting 3-D velocity dataset was converted into a bidirectional velocity map in an en face (x-y) plane with its depth projection in amplitude. However, DOMAG can represent the true flow velocity at diving arterioles and ascending venules in the cortex within the limited velocity range because these penetrating vessels are almost in parallel to the incident OCT beam (i.e., the angle between the OCT beam and blood flow direction is close to zero). Therefore, it is effective for detecting flow in the descending arteriole feeding blood supply to the underlying capillaries [32],

D. Attenuation coefficient

As coherent light such as OCT light propagates through a turbid medium, the power of the light beam is exponentially attenuated along its propagating path due to progressive scattering and absorption of light. The attenuation depends on the intrinsic optical property of the medium and is entirely governed by the attenuation coefficient (combined absorption and scattering) for a low NA optics. The determination of the attenuation coefficient from the OCT measurements is, therefore, useful in characterizing the optical property of the medium.

In ischemic stroke, it is well known that energy depletion in neuronal cells following cerebral ischemia induces loss of cellular integrity and function [33]. We assumed that the pathophysiology of cerebral ischemia would change the composition of the ischemic tissue, resulting in altered attenuation [23]. To interpret the brain tissue characteristics, we measured attenuation coefficients by analyzing the OCT depth profiles. Rather than using a classical exponential curve-fitting method [34], we employed a method based on a single scattering model, proposed by Vermeer *et al* [35], to determine the depth-resolved attenuation coefficients from the OCT depth profiles. This method can estimate attenuation coefficients at each pixel of the OCT depth profiles. The mapping of localized, per-pixel attenuation coefficients can provide a comprehensive interpretation of the optical property changes in a heterogeneous multi-layered tissue such as the cerebral cortex. According to Vermeer *et al* [35], the attenuation coefficient corresponding to a certain pixel can be expressed as:

$$\mu[i] = I[i] / \left(2\Delta \sum_{i+1}^{\infty} I[i]\right), \quad (4)$$

where $I[i]$ denotes the OCT signal amplitude at the i-th pixel along the depth and Δ is the axial length of pixel. In spectral domain OCT, however, the sensitivity drops with imaging depth due to a limited resolution of the spectrometer and aliasing at high spatial frequencies resulting from the discrete sampling by the line scan camera with finite pixel numbers. This systematic signal decay (sensitivity roll-off) may affect the OCT signal directly due to the optical properties of the sample. In order to compensate for the depth-dependent signal decay before an estimation of the attenuation coefficient, the sensitivity roll-off $H(z)$ was measured. Point spread functions (PSFs) were recorded by displacing the reflective mirror surface at a series of imaging depths in the axial (z) direction and then the peak amplitudes of PSFs were simply fit as a Gaussian function [35]:

$$H(z) = \exp\left(-z^2/\sigma^2\right), \quad (5)$$

where σ is the width of the Gaussian function determined from the sensitivity measurement. Eventually, each A-line was divided by this signal decay factor, and the resulting corrected A-line signals were used for the calculation of the attenuation coefficient. Fig. 1E shows the measured sensitivity roll-off of our SD-OCT system, showing a 3-dB loss at the 270-th pixel corresponding to a depth of 1 mm in the brain tissue (refractive index 1.35 [36]). The pre-

compensation attenuation coefficient image of Fig. 1A is shown in Fig. 1C. After compensation using the fitting function of sensitivity roll-off in Fig. 1E, the corrected image (Fig. 1D) had relatively low attenuation values, which were identified in comparison to the depth profiles (taken at the white lines in Figs. 1C and 1D) in Fig 1F. The average attenuation coefficient (4.91 mm^{-1}) in the white matter (a gray shadow in Fig. 1F) was much higher compared to that (1.01 mm^{-1}) in the gray matter, which is consistent with previous results obtained with 6–14 week-old CD1 mice with a thinned-skull cortical window using a 1300 nm SD-OCT system [37]. This large attenuation might be caused by high scattering of a bundle of myelinated axons in the white matter [38]. Fig. 1I shows an attenuation coefficient map of the mouse cortex, corresponding to both the structure (Fig. 1G) and vasculature (Fig. 1H) maps.

E. Cerebral blood flow

However, it is unlikely that an absolute CBF threshold for tissue infarction exists. Hence, the CBF reduction has been usually measured with a relative CBF (rCBF) that is represented as a percentage of the baseline CBF value in the targeted cortex, useful for evaluating the outgrowth of the cerebral infarct [39][40][19]. We calculated rCBF using the acquired vascular maps (angiograms), with the assumption that the OCTA signal is proportional to the CBF. This is a reasonable assumption, as the perfusion signals obtained by OMAG approach have a linear relationship with blood flow (volume/time), a product of blood flow velocity (mm/time) and RBC flux (cells/time) [41]. Please note here that DOMAG measurement in Section III.C is the axial component of blood flow velocity. We hypothesized that from the focal perfusion deficit caused by distal MCA occlusion, the hypoperfused area would develop in a radial fashion (see Fig. 2A). With this hypothesis, we drew and plotted a total of 500 concentric circles with a given center position but different radii on the angiogram and then the pixels within the perimeter of each circle were taken and their amplitudes were averaged. The center of the circles was determined using the ischemic territory in the angiogram at a certain time point, whose border line was assumed to be a portion of the circumference. Therefore, the average value at the *i-th* circle was divided by an average at the same order of circle in the pre-occlusion baseline angiogram, yielding a relative perfusion signal change to the baseline, representing rCBF. We note that all angiograms including the baseline were co-registered using an automatic image registration technique [42] prior to the rCBF calculation. The calculated rCBF value (%) was remapped to all pixels in the circle perimeter, making the entire circle have the same rCBF value. Consequently, the angiogram was converted to a concentric distribution of the blood flow reduction by remapping the respective rCBF value to each circle. Fig. 2B shows rCBF in color, overlaid on the grayscale angiogram 90 minutes post-dMCAO. A rCBF profile (Fig. 2C) taken along a white dotted line in Fig. 2B displays a distinct blood flow reduction, with the distance from the center of the circles and in the evaluated regions, specifically, flow ranges > 92 % for the unaffected normal region (N); 66–92 % for the region of mild hypoperfusion, referred to as benign oligemia (BO); 38–66 % for the peri-infarct region, penumbra (P); and 0–38 % for the infarct core (IC) [19].

IV. Experimental results

A. Acute changes in cerebral blood perfusion and velocity post dMCAO

In order to observe changes in cerebral blood perfusion in the early ischemic brain, serial OMAG and DOMAG measurements were performed on the mouse brain (n=5) every 2 minutes for 3 hours. Figure 3 describes the time-course of the OMAG (Fig. 3A) and DOMAG (Fig. 3B) images for one animal, representing the perfusion maps and blood flow axial velocity maps, respectively. In the OMAG images, the significant blood flow reduction in the MCA branches (arrows), resulting from the occlusion of the distal MCA, led to perfusion drop in capillaries, and the hypoperfused area extended slightly over time (~130 minutes). However, simultaneously, we also observed a similar capillary nonperfusion in the ACA (arrow head) area, away from the ischemic brain region, where capillary perfusion started to reduce from the proximal ACA toward the cerebral collaterals (at roughly '8:00 o'clock' in the OMAG images at 14, 16, and 40 minutes) and then the drop in perfusion persisted for almost 20 minutes (data not shown). Afterwards, interestingly, perfusion slowly recovered toward the baseline level (again, at '8:00 o'clock' in the OMAG image at 64, 78, 98, and 114 minutes). The perfusion dynamics are shown in animation in Movie 1.

The DOMAG images in Fig. 3B show the time course changes in RBC axial flow velocities in the surface pial vessels and the penetrating vessels rather than the capillaries. The DOMAG signals are coded with gradient colors that indicate the velocity scale, in a range from − 6.1 mm/s to 6.1 mm/s. The diving arterioles and rising venules are indicated by the discrete green and red colors, respectively. One can see that the flow velocities at the penetrating vessels continuously decreased in the ischemic brain, whilst the penetrating flow velocities in the non-ischemic ACA region gradually reverted to the baseline, similar to the capillary perfusion responses in the OMAG images. Because penetrating arterioles play a key role in distributing pial arterial flow into the downstream capillary network, the disruption of blood flow in the penetrating arterioles significantly affects the capillary density observed in the corresponding OMAG images. The hemodynamics in the non-ischemic and ischemic brain is highlighted in the small region of interest (ROI) sites (1 mm × 1 mm) of the OMAG and DOMAG images (orange and red dotted boxes) as shown in Fig. 3C and Fig. 3D, respectively.

B. Acute changes in cerebral blood flow post dMCAO

We investigated the percentage change of CBF relative to baseline values (rCBF) after dMCAO. The spatial distribution of rCBF post-dMCAO were displayed in false-color on the corresponding OMAG images (Fig. 4A). Warmer colors correspond to higher percentages of the baseline CBF. Visually, it is apparent that as a result of the dMCAO, the CBF following acute ischemia exhibited two distinct responses, based on cortical location. In the ischemic region close to the occluding MCA site, the rCBF level monotonically declined (becoming increasingly bluer), while the rCBF level in the non-ischemic region near the ACA initially decreased (shifting from red to yellow), which then gradually recovered toward the baseline.

The time courses of the relative changes in CBF at three spatial locations, P1, P2, and P3, were measured for each mouse (n=5) and are shown in Fig. 4B. The three locations were 2.5

mm, 3.5 mm, and 4.5 mm away from the occlusion site, with a 1 mm gap between the locations (see photograph in Fig. 4A). The rCBF curves at PI (closest to the focal occlusion) indicate that. CBF declined significantly, to ~60 % of the baseline value (penumbra) within a few minutes after arterial occlusion, and declined further, to below 20 % of baseline (infarct core), within 3 hours post-occlusion. Likewise, the rCBF curves at P2 (close to the focal perfusion deficit) show a CBF reduction from 70 % to ~35 % of baseline for 3 hours, corresponding to the CBF thresholds of benign oligemia to ischemic penumbra in acute ischemic stroke. However, the rCBF curves at P3 (farthest from the focal perfusion deficit) commonly exhibited a characteristic concave-up shape in the 3-hour time window, in which CBF declined to ~70 % within 25 minutes post dMCAO and after a 20-minute plateau in the CBF perfusion, CBF was gradually restored to 90 % of baseline. This change in rCBF was varied in the CBF threshold range of the benign oligemia (66–92 % of baseline) [19]. The changes observed in rCBF are animated in a video sequence (Movie 2).

C. Acute changes in attenuation coefficients post dMCAO

The time-course attenuation coefficient maps demonstrate the change in cortical tissue scattering properties post-dMCAO, as shown in Fig. 5A. We observed an increase in the attenuation coefficient ($> 3\ mm^{-1}$) in the cortical region around the focal ischemia (right lateral side in Fig. 5A) and its spatial expansion over time as the cerebral ischemia progressed. It clearly indicates that the cortical scattering properties on the lateral side changed. In particular, we found that the rim of the cortical area (arrow heads in Fig. 5A) appeared 8 minutes after dMCAO and manifested with significantly higher attenuation coefficients ($> 4.5\ mm^{-1}$), expanding over time. This distinct border zone demarcated the region with intermediate brightness in the attenuation coefficient, (right lateral side in Fig. 5A). Figure 5B shows an overlay of the OMAG image (red) and the attenuation coefficient map (green) 130 minutes post-dMCAO. A boundary of the non-perfused area spatially correlates to the border zone of the attenuation coefficient. This correlation indicates that the ischemic brain is characterized by changes in blood perfusion as well as light scattering of cortical tissue. TTC staining was performed on the harvested mouse brains at the terminal point for OCT imaging (130 minutes post dMCAO) to examine cerebral injury. The stained brain slices are shown reassembled in Fig. 5C. In this histological assessment, the absence of TTC staining characterizes “infarcted” tissue, and the regions identified as core and viable tissue is stained pink or red [43]. We identified co-registration of the attenuation border zone and the boundary of white area (infarct core) in the TTC-stained brain. Therefore, this finding suggests that the infarction might be easily identified by locating the strong white band in the time-dependent attenuation coefficient map. The changes detected in the attenuation coefficients are animated as a video sequence in Movie 3.

In comparison with the OMAG images, we also observed displacement of penetrating vessels in the ischemic brain proximal to the MCA, characterized by high attenuation coefficients ($> 3\ mm^{-1}$) in the attenuation coefficient maps. Figure 5D demonstrates the movement of a penetrating vessel in a small ROI (white box in Fig. 5B) after transient MCA occlusion, where two penetrating arterioles (arrows) were progressively shifted, appearing left-folded in the OMAG images. The displacement, was represented as the difference in the angle between the pial branch and its penetrating vessel, relative to baseline. Figure 5E show

an angle deviation over ~17 degrees on average for five mice, while the deviation was marginal (< 3 degrees) relative to the penetrating vessels in the ACA region. This observation from comparing the OMAG and attenuation coefficient measurements suggests an involvement of vessel migration in the ischemic damage to the brain.

V. Discussion and conclusion

We have described here a multi-parametric optical coherence tomography (OCT) approach to investigate cerebral tissue injury progression and blood flow impairment in the early stages of ischemic stroke in a mouse dMCAO model *in vivo*. Multi-parametric OCT imaging provided a range of endogenous contrasted images using intrinsic optical scattering properties of RBCs and cortical tissues, offering depth-resolved information regarding cerebral vasculature, blood flow velocity, CBF, and tissue property change in mouse brain. This OCT approach was used for time-course monitoring of focal ischemic stroke in mice, through an open-skull cranial window with a recording time interval of 2 minutes. During the acute stage (first 3 hours) after dMCAO, we revealed a spatiotemporal relationship between hemodynamics and tissue scattering change across the mouse cortex (4 mm × 4 mm), providing new insights on the hemodynamic events associated with pathogenesis of tissue infarction and penumbra development after ischemic insult.

The OMAG imaging demonstrated its capability to monitor capillary perfusion, penetrating vessel velocity and CBF in cortical tissue. In all mice (n=5), immediately after dMCAO, a significant capillary perfusion drop occurred along with constrictive vessel tone in the MCA branches within a few minutes, with a clearly defined region devoid of perfused capillaries that eventually formed a border between the capillary-perfused tissue and the capillary non-perfused tissue. While the previous OCT angiography studies have only reported the capillary non-perfusion in ischemic core, [19]–[24] we here revealed additional blood flow behaviors in the regions proximal and distal to the origin of insult. For instance, OMAG angiogram in Fig. 3C and 3D illustrated two distinct capillary perfusion dynamics at anterior cerebral artery (ACA) territory and MCA territory. While a progressive capillary perfusion drop was developed in MCA territory after dMCAO, capillary vessels in ACA territory exhibit a short period of compromised flow perfusion at first, followed by a recovery to its baseline level. Moreover, DOMAG results of these two regions showed synchronous change of penetrating vessel velocity map (Fig. 3C and 3D) compared to its downstream capillary perfusion, validating the important role of penetrating arteriole in supplying downstream capillary bed.

In addition to angiogram and flow velocity map, propagation of CBF decline was also observed from the relative CBF (rCBF, relative change in CBF to baseline) maps estimated from OMAG amplitudes (Fig. 4A). Interestingly, CBF in the ACA territory fell to 70 % of baseline within ~25 minutes after dMCAO and this level persisted for ~20 minutes, then gradually elevated up to 90 % of baseline at about 2 hours (see the line plot at P3 in Fig. 4B). It is currently unclear about the underlying mechanism of the distinct hemodynamic response in ACA region during dMCAO. The earlier study of embolic stroke model of rat has reported the similar CBF response that was monitored using laser speckle flowmetry during focal ischemia [44] although the study has revealed periodic CBF waves (appeared as

small hyperemic peaks) coupled to cortical spreading depolarizations that was not apparently seen in our result.

The light attenuation mapping demonstrated the changes in tissue scattering in the cerebral cortex. In this study, TTC staining was performed to guide the region definition for the interpretation of *in vivo* OCT results. In Fig. 5A, a notable increase in the attenuation coefficient value was observed in the capillary non-perfused area, which were later confirmed as tissue infarction. A possible explanation to the increase in attenuation coefficient, hence the increase scattering in the ischemic region, is excitotoxicity, a putative cascade of damaging events in focal cerebral ischemia evolving too quickly that is lethal to neuron and glia cells, eventually leading to cell death (cell necrosis) [45], Indeed, the increased scattering signature from the necrotic tissue has been reported in the previous OCT study for imaging of tissue viability [23][46]. However, the ischemic injury may also entail vasogenic edema that occurs over the first few hours after the onset of a focal perfusion deficit [47], The formation of brain vasogenic edema increases brain microvascular permeability, causing considerable movement of vascular fluid across the capillary endothelium, resulting in an influx of extracellular fluid into the ischemic lesion. Consequently, the accumulation of excess fluid can induce scattering decrease in the stroke core [37], From our imaging results (Fig. 5A), therefore, we suppose that the increase in attenuation caused by the cell necrosis may be compromised with the effect of cerebral edema. The contribution of two cascade events (cell necrosis and edema) will need further systematic investigation, preferably with histochemistry, for observation of cell morphology [23] and brain water content analysis using wet-dry method [48].

Furthermore, a new finding in our study revealed a higher-attenuation coefficient border zone along the ischemic region, expanding during infarct progression (Fig. 5A). One possible explanation for the highly scattering boundary is the effect of vasogenic edema mentioned above [47]. During focal stroke, the space-occupying effect of edema may push die adjacent brain structures involving the penetrating vessels and capillaries into the lateral directions. Accordingly, the vessels would be increasingly shifted along with the brain structures being mechanically displaced (Fig. 5D) due to the elevated pressure by edema, thereby leading to mechanical compression of the brain compartments including neurons, nerve tracts, and cerebral vessels [47]. Eventually, the surrounding brain tissues would become much denser and the optical scattering in the compressed tissues would increase, reflected by the higher attenuation coefficients. However, direct observation of the displacement of the brain structures in OCT cross-sections is challenging because of strong speckle artifacts generated by the multiply-scattered lights due to heterogeneous cortical tissues, hiding the light scattering from the brain compositions. The displacement can be inferred from the lateral transition and expansion of the attenuation increase in Fig. 5F.

It is also worth to note that in each animal (n=5), the highly attenuated region was spatially correlated with the infarct core defined by TTC-stained brain (Fig. 5C), which was also co-registered with the capillary non-perfused region in the angiogram (Fig. 5B). Our finding is similar to the results from the previous OCT stroke studies. For example, Srinivasan *et al* [23] identified that the capillary non-perfusion during focal stroke correlated spatially with the scattering increase and the scattering alteration was co-registered with the infarcted area

with no MAP2 immunoresponse (the absent immunoreactivity of MAP2 indicates the infarction). Also, a recent work by Yang *et al* [24] demonstrated the spatial correlation between capillary non-perfusion and the increase in scattering during the photo-thrombotic focal ischemia. This discovery together with the hemo-dynamic feature visualization opens a new possibility of multi-parametric OCT to identify early the infarct border and evaluate penumbral region *in vivo* without sacrificing animal. Such unique and comprehensive ability of OCT may provide guidance to the pharmacologic or surgical intervention that aims to salvage ischemic penumbra; thus, reducing infarct size.

In conclusion, we have demonstrated a novel OCT imaging platform for spatiotemporal dynamic imaging of vascular and cellular responses to brain injury after acute ischemic stroke. The ability of efficiently monitoring multiple physiologic events *in vivo*would allow an in-depth investigation into the mechanisms underlying ischemic brain damage in pre-clinical studies and facilitate the development of adequate therapeutic strategies to improve the prognosis of ischemic stroke.

Supplementary Material

Refer to Web version on PubMed Central for supplementary material.

Acknowledgments

This work is supported by The National Heart, Lung, and Blood Institute (ROI HL093140), the National Eye Institute (ROI EY024158), Washington Research Foundation, WRF David and Nancy Auth Innovation Award, and an unrestricted fund from Research to Prevent Blindness. The funding organization had no role in the design or conduct of this research.

References

[1]. Baron JC, “Perfusion thresholds in human cerebral ischemia: historical perspective and therapeutic implications,” Cerebrovasc. Dis, vol. 11, suppl. 1, pp. 2–8, 2 2001.

[2]. Lee DH, Kang D-W, Ahn JS, Choi CG, Kim SJ, and Suh DC, “Imaging of the ischemic Penumbra in acute stroke,” Korean J. Radiol, vol. 6, no. 2, pp. 64–74, 6 2005. [PubMed: 15968144]

[3]. Ramos-Cabrer P, Campos F, Soibino T, Castillo J, “Targeting the ischemic penumbra,” Stroke, vol. 42, suppl. 1, pp. S7–11, 1 2011. [PubMed: 21164112]

[4]. Liu R, Yuan H, Yuan F, and Yang SH, “Neuroprotection taigeting ischemic penumbra and beyond for the treatment of ischemic stroke,” Neurol. Res, vol. 34, no. 4, pp. 331–337, 5 2012. [PubMed: 22643076]

[5]. Marchal G, Serrati C, Rioux P, Petit-Taboue MC, Viader F, de la Sayette V, Le Doze F, Lochon P, Derlon JM, Orgogozo JM et al., “PET imaging of cerebral perfusion and oxygen consumption in acute ischaemic stroke: relation to outcome,” Lancet, vol. 341, no. 8850, pp. 925–927, 4 1993. [PubMed: 8096267]

[6]. Schaefer PW, Hunter GJ, He J, Hamberg LM, Sorensen AG, Schwamm LH, Koroshetz WJ, Gonzalez RG, “Predicting cerebral ischemic infarct volume with diffusion and perfusion MR imaging,” AJNR Am. J. Neuroadiol, vol. 23, no. 10, pp. 1785–1794, 12 2002.

[7]. Abels B, Klotz E, Tomandi BF, Kloska SP, Lell MM, “Perfusion CT in acute ischemic stroke: a qualitative and quantitative comparison of deconvolution and maximum slope approach,” AJNR Am. J. Neuro-raaiol, vol. 31, no. 9, pp. 1690–1698, 10 2010.

[8]. Heiss WD, and Sobesky J, “Comparison of PET and DW/PW-MRI in acute ischemic stroke,” Keio J. Med, vol. 57, no. 3, pp. 125–131, 9 2008. [PubMed: 18854664]

[9]. Heiss WD, “Radionuclide imaging in ischemic stroke,” J. Nucl. Med, vol. 55, no. 11, pp. 1831–1841, 11 2014. [PubMed: 25300599]

[10]. Warach S, “Measurement of the ischemic penumbra with MRI: it’s about time,” Stroke, vol. 34, no. 10, pp. 2533–2534, 10 2003. [PubMed: 12970511]

[11]. Schlaug G, Benfield A, Baird AE, Sieweit B, Lovblad KO, Parker RA, Edelman RR, and Warach S, ‘The ischemic penumbra: operationally defined by diffusion and perfusion MRI,” Neurology, vol. 53, no. 7, pp. 1528–1537, 10 1999. [PubMed: 10534263]

[12]. Kidwell CS, Alger JR, and Saver JL, “Beyond mismatch: evolving paradigms in imaging the ischemic penumbra with multimodal magnetic resonance imaging,” Stroke, vol. 34, no. 11, pp. 2729–2735, 11 2003. [PubMed: 14576370]

[13]. Fisher M, Ginsberg M, “Current concepts of the ischemic penumbra. Introduction,” Stroke, vol. 35, no. 11, pp. 2657–2658, 11 2004.

[14]. Tomlins PH, Wang RK, “Theory, developments and applications of optical coherence tomography.” J. Phys. D: Appl. Phys Vol. 38, no. 15, pp. 2519–2535, 2015.

[15]. Choi WJ, Reif R, Yousefi S, and Wang RK, “Improved microcirculation imaging of human skin in vivo using optical microangiography with a correlation mapping mask,” J. Biomed. Opt, vol. 19, no. 3, pp. 36010, 3 2014. [PubMed: 24623159]

[16]. Wang RK, An L, “Doppler optical microangiography for volumetric imaging of vascular^{-} perfusion in vivo” Opt. Express, vol. 17, no. 11, pp. 8926–8940, 5 2009. [PubMed: 19466142]

[17]. Baran U, Li Y, and Wang RK, “In vivo tissue injury mapping using optical coherence tomography based methods,” Appl. Opt, vol. 54, no. 21, pp. 6448–6453, 7 2015. [PubMed: 26367827]

[18]. Iliff JJ, Wang RK, Zeldin DC, Alkayed NJ, “Epoxyeicosanoids as Mediators of Neurogenic Vasodilation in Cerebral Vessels”, Am. J. Physiol. - Heart Circ. Physiol, vol.296, pp. 1352–1363, 2009.

[19]. Dziennis S, Qin J, Shi L, and Wang RK, “Macro-to-micro cortical vascular imaging underlies regional differences in ischemic brain,” Sci. Rep, vol. 5, pp. 10051, 5 2015. [PubMed: 25941797]

[20]. Jia Y, and Wang RK, “Optical micro-angiography images structural and functional cerebral blood perfusion in mice with cranium left intact,” J. Biophotonics, vol. 4, no. 1–2, pp. 57–63, 1 2011. [PubMed: 20183828]

[21]. Wang RK, Jacques SL, Ma Z, Hurst S, Hanson SR, and Gruber A, “Three dimensional optical angiography,” Opt. Express, vol. 15, no. 7, pp. 4083–4097, 4 2007. [PubMed: 19532651]

[22]. Lee J, Gursoy-Ozdemir Y, Fu B. Boas DA, and Dalkara T, “Optical coherence tomography imaging of capillary reperfusion after ischemic stroke,” Appl. Opt, vol. 55, no. 33, pp. 9526–9531, 11 2016. [PubMed: 27869849]

[23]. Srinivasan VJ, Mandeville ET, Can A, Blasi F, Climov M, Daneshmand A, Lee JH, Yu E, Radhakrishnan H, Lo EH, Sakadzic S, Eikermann-Haerter K, Ayata C, “Multiparametric, longitudinal optical coherence tomography imaging reveals acute injury and chronic recovery in experimental ischemic stroke,” PLoS One, vol. 8, no. 8, pp. e71478, 8 2013. [PubMed: 23940761]

[24]. Yang S, Liu K, Ding H, Gao H, Zheng X, Ding Z, Xu K, and Li P, “Longitudinal in vivo intrinsic optical imaging of cortical blood perfusion and tissue damage in focal photothrombosis stroke model,” J. Cereb. Blood Flow Metab, DOI: 10.1177/0271678X18762636, 2 2018.

[25]. Li Y, Baran U, and Wang RK, “Application of thinned-skull cranial window’ to mouse cerebral blood flow’ imaging using optical microangiography,” PLoS One, vol. 9, no. 11, pp. el 13658, 11 2014.

[26]. Llovera G, Roth S, Plesnila N, Veltkamp R, and Liesz A, “Modeling stroke in mice: permanent coagulation of the distal middle cerebral artery,” J. Vis. Exp, no. 89, pp. e51729, 7 2014.

[27]. Choi WJ, Zhi Z, and Wang RK, “In vivo OCT microangiography of rodent iris,” Opt. Lett, vol. 39, no. 8, pp. 2455–2458, 4 2014. [PubMed: 24979017]

[28]. An L, Qin J, and Wang RK, “Ultrahigh sensitive optical microangiography for in vivo imaging of microcirculations within human skin tissue beds,” Opt. Express, vol. 18, no. 8, pp. 8220–8228, 4 2010. [PubMed: 20588668]

[29]. Xu J, Song S, Li Y, and Wang RK, “Complex-based OCT angiography algorithm recovers microvascular information better than amplitude-or phase-based algorithms in phase-stable systems,” Phys. Med. Biol, vol. 63, no. 1, pp. 015023, 12 2017. [PubMed: 29049034]

[30]. Berbel P, Navarro D, Auso E, Varea E, Rodriguez AE, Ballesta JJ, Salinas M, Flores E, Faura CC, and de Escobar GM, “Role of late maternal thyroid hormones in cerebral cortex development: an experimental model for human prematurity,” Cereb. Cortex, vol. 20, no. 6, pp. 1462–1475, 6 2010. [PubMed: 19812240]

[31]. Shi L, Qin J, Reif R, and Wang RK, “Wide velocity range Doppler optical microangiography using optimized step-scanning protocol with phase variance mask,” J. Biomed. Opt, vol. 18, no. 10, pp. 106015, 10 2013. [PubMed: 24165741]

[32]. Baran U, Li Y, and Wang RK, “Vasodynamics of pial and penetrating arterioles in relation to arteriolo-arteriolar anastomosis after focal stroke,” Neurophotonics, vol. 2, no. 2, pp. 025006, 4 2015. [PubMed: 26158010]

[33]. Bramlett HM, and Dietrich WD, “Pathophysiology of cerebral ischemia and brain trauma: similarities and differences,” J. Cereb. Blood Flow Metab, vol. 24, no. 2, pp. 133–150, 2 2004. [PubMed: 14747740]

[34]. Chong SP, Merkle CW, Cooke DF, Zhang T, Radhakrishnan H, Krubitzer L, and Srinivasan VJ, “Noninvasive, in vivo imaging of subcortical mouse brain regions with 1.7 μm OCT,” Opt. Lett, vol. 40, no. 21, pp. 4911–4914, 11 2015. [PubMed: 26512481]

[35]. Vermeer KA, Mo J, Weda JJA, Lemij HG, and de Boer JF, ‘Depth-resolved model-based reconstruction of attenuation coefficients in OCT,” Biomed. Opt. Express, vol. 5, no. 1, pp. 322–337, 12 2014.

[36]. Binding J, Arous JB, Léger J-F, Gigan S, Boccara C, and Bour-dieu L, “Brain refractive index measured in vivo with high NA defocus-corrected full-field OCT and consequences for two-photon microscopy,” Opt. Express, vol. 19, no. 6, pp. 4833–4847, 3 2011. [PubMed: 21445119]

[37]. Rodriguez CLR, Szu JI, Eberle MM, Wang Y, Hsu MS, Binder DK, and Park BH, “Decreased light attenuation in cerebral cortex during cerebral edema detected using optical coherence tomography,” Neurophotonics, vol. 1, no. 2, pp. 025004, 10 2014. [PubMed: 25674578]

[38]. Wang H, Magnain C, Sakadžić S, Fischl B, and Boas DA, “Characterizing the optical properties of human brain tissue with high numerical aperture OCT” Biomed. Opt. Express, vol. 8, no. 12, pp. 5617–5636, 11 2017. [PubMed: 29296492]

[39]. Liu Y, Karonen JO, Vanninen RL, Ostergaard L, Roivainen R, Nuutinen J, Perkiö J, Könönen M, Hämäläinen A, Vanninen EJ, Soimakallio S, Kuikka JT, and Aronen HJ, “Cerebral hemodynamics in human acute ischemic stroke: a study with diffusion- and perfusion-weighted magnetic resonance imaging and SPECT,” J. Cereb Blood Flow Metab, vol. 20, no. 6, pp. 910–920, 6 2000. [PubMed: 10894174]

[40]. Luo W, Wang Z, Li P, Zeng S, and Luo Q, “A modified mini-stroke model with region-directed reperfusion in rat cortex,” J. Cereb. Blood Flow Metab, vol. 28, no. 5, pp. 973–983, 5 2008. [PubMed: 18073774]

[41]. Choi WJ, Qin W, Chen CL, Wang J, Zhang Q, Yang X, Gao BZ, and Wang RK, “Characterizing relationship between optical microangiography signals and capillary flow using microfluidic channels,” Biomed. Opt. Express, vol. 7, no. 7, pp. 2709–2728, 6 2016. [PubMed: 27446700]

[42]. Wei DW, Deegan AJ, and Wang RK, “Automatic motion correction for in vivo human skin OCTA through combined rigid and nonrigid registration,” J. Biomed. Opt, vol. 22, no. 6, pp. 66013, 6 2017. [PubMed: 28636065]

[43]. Liu F, Schafer DP, and McCullough LD, “TTC, fluoro-Jade B and NeuN staining confirm evolving phases of infarction induced by middle cerebral artery occlusion,” J. Neurosci. Methods, vol. 179, no. 1, pp. 1–8, 4 2009. [PubMed: 19167427]

[44]. Kumagai T, Walberer M, Nakamura H, Endepols H, Sué M, Vollmar S, Adib S, Mies G, Yoshimine T, Schroeter M, and Graf R, ‘Distinct spatiotemporal patterns of spreading depolarizations during early infarct evolution: evidence from real-time imaging,” J. Cereb Blood Flow Metab, vol. 31, no. 2, pp. 580–592, 2 2011. [PubMed: 20700132]

[45]. Deb P, Sharma S, and Hassan KM, “Pathophysiologic mechanisms of acute ischemic stroke: an overview with emphasis on therapeutic significance beyond thrombolysis,” Pathophysiology, vol. 17, no. 3, pp. 197–218, 6 2010. [PubMed: 20074922]

[46]. Vakoc BJ, Lanning RM, Tyrrell JA, Padera TP, Bartlett LA, Stylianopoulos T, Munn LL, Tearney GJ, Fukumura D, Jain RK, and Bouma BE, ‘Three-dimensional microscopy of the tumor microenvironment in vivo using optical frequency domain imaging,” Nat. Med, vol. 15, no. 10, pp. 1219–1223, 10 2009. [PubMed: 19749772]

[47]. Gerriets T, Walberer M, Ritschel N, Tschematsch M, Mueller C, Bachmann G, Schoenburg M, Kaps M, and Nedelmann M, “Edema formation in the hyperacute phase of ischemic stroke. Laboratory investigation,” J. Neurosurg, vol. Ill, no. 5, pp. 1036–1042, 11 2009.

[48]. Schwab M, Bauer R, and Zwiener U, “The distribution of normal brain water content in Wistar rats and its increase due to ischemia,” Brain Res, vol. 749, no. 1, pp. 82–85, 2 1997. [PubMed: 9070630]

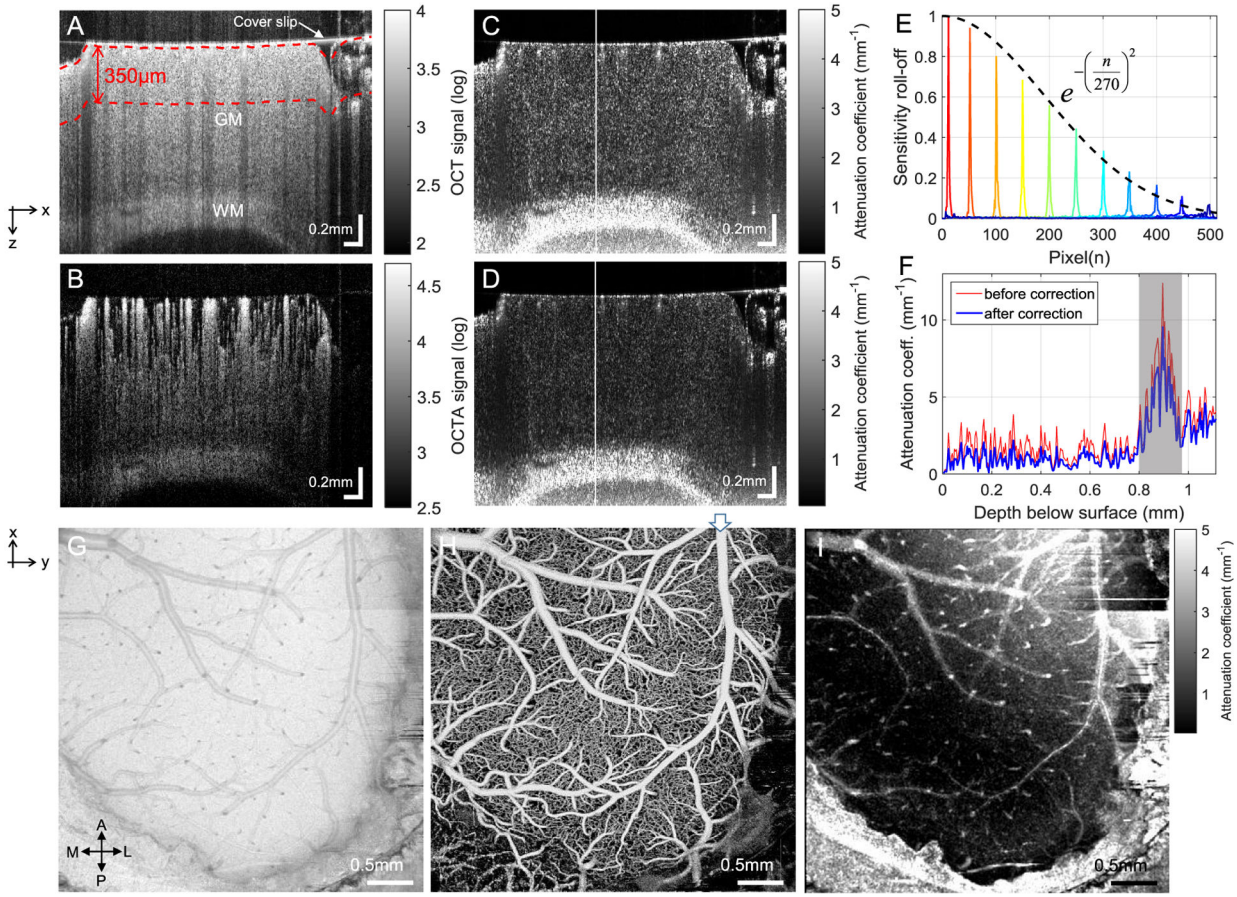

Fig. 1.

In vivo OCT imaging of a healthy mouse brain with cranial window preparation. (A) Cross-sectional (x-z) OCT image (logarithmic scale), describing anatomical details of the cerebral cortex; gray matter (GM) and white matter (WM). (B) Corresponding cross-sectional (x-z) OCTA image (logarithmic scale), representing blood perfusion in the cortex. (C) Corresponding cross-sectional attenuation coefficient image before compensation for the depth-dependent signal decay. The correction was made with a fitting function $H(z)$ (dotted line) of the peak amplitudes of normalized sensitivity roll-off signals of the SD-OCT system in (E), and thus a resulting compensated image is seen in (D). (F) Comparison of the attenuation depth profiles (white lines in (C) and (D)) exhibits the lowered values in attenuation coefficients after compensation. The region marked with gray shadow indicates the location of white matter (WM) having significantly higher attenuation coefficients. Maximum amplitude projections (MAPs) of 3-D OCT, OCTA and attenuation coefficients taken over the depth of 350 μm below the cortical surface (between two red dotted lines in (A)) display the structural map (G), vascular map (H), and attenuation coefficient map (I), respectively.

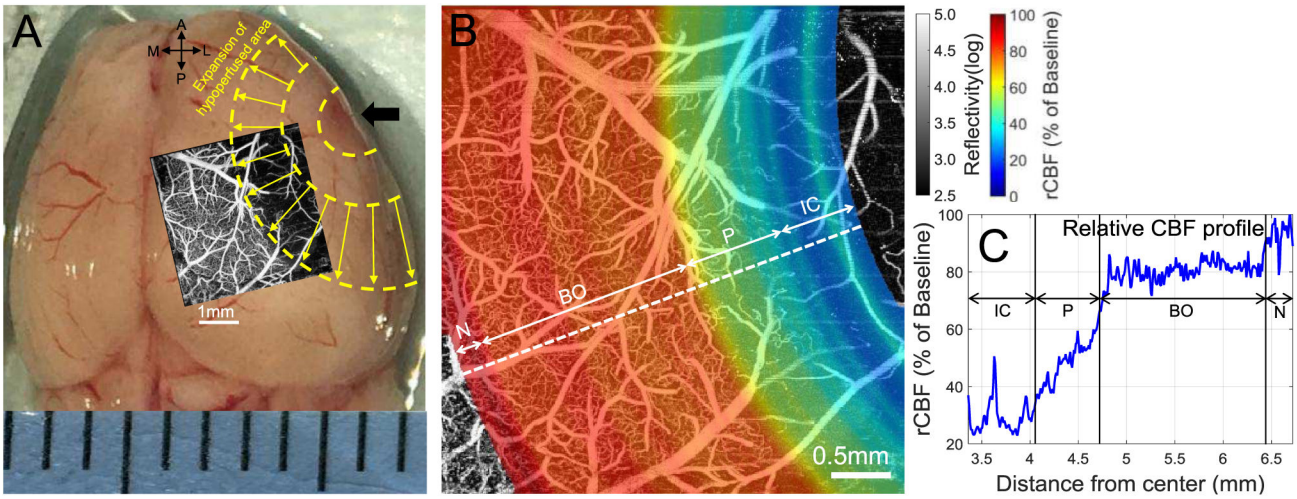

Fig. 2.

Relative cerebral blood flow (rCBF) measurement. (A) Photographic image of a stroke brain harvested 2.5 hours post-dMCAO. Arrow indicates the blood occluded site of the brain. An angiogram (inset) obtained at 1.5 hours post-dMCAO is co-localized with the brain where the ischemic area would be expanded in space with a concentric pattern indicated as yellow dotted semicircles. (B) Spatial distribution of the rCBF in color, overlaid with the angiogram at 1.5 hours post dMCAO. (C) Profile of the rCBFs, with distance from the blood occlusion site. IC, infarct core; P, penumbra; BO, benign oligemia; N, normal.

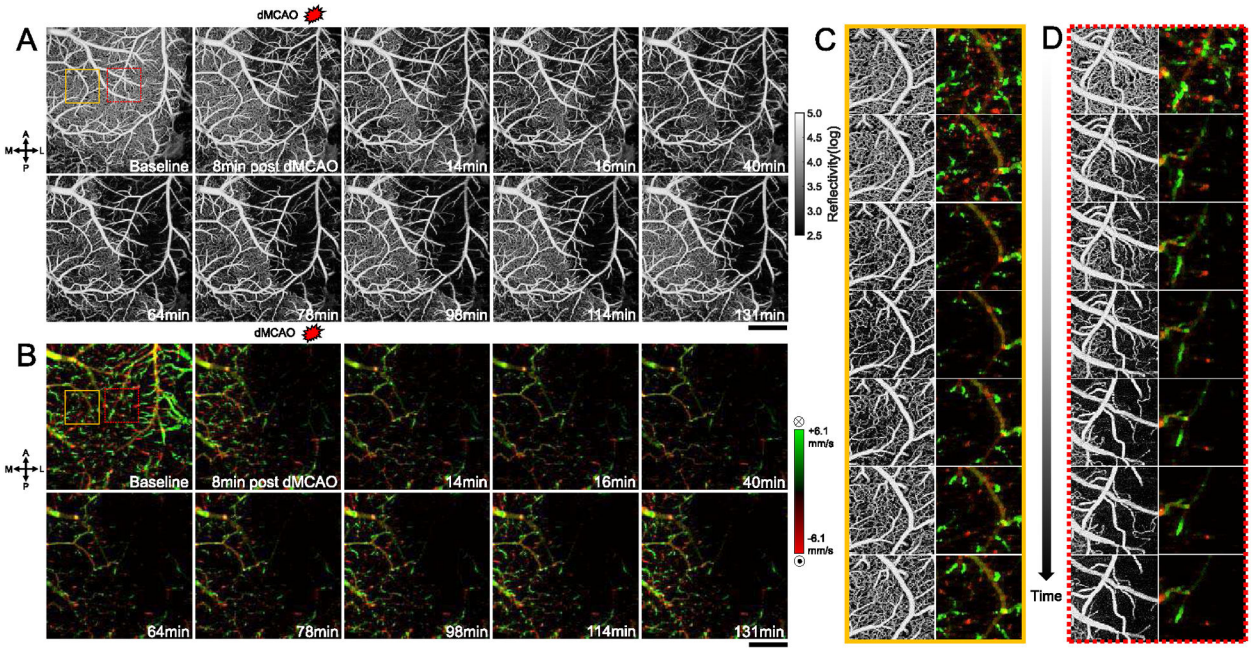

Fig. 3.

Representative time-sequences of OMAG and DOMAG images illustrating synchronous changes in blood perfusion and blood flow velocity in the cerebral cortex of young adult mouse with cranial window preparations. (A) OMAG images demonstrate change in cerebral blood perfusion from baseline to 131 minutes after dMCAO. The scale to the right represents a logarithmic gray scale in reflectivity. (B) Pseudo-colored DOMAG images show bidirectional axial components of RBC flow velocities in cerebral vessels. The red color in (B) represents blood moving toward the incident probe beam (negative direction), with the green color representing the opposite (positive) direction; their color tones indicate the velocity, which extends from −6.1 mm/s to +6.1 mm/s. Scale bars are 1 mm. The dynamic changes in the perfusion and velocity of blood flow were clearly observed in the small region (1 mm × 1 mm) proximal to ACA (C) and MCA (D), respectively.

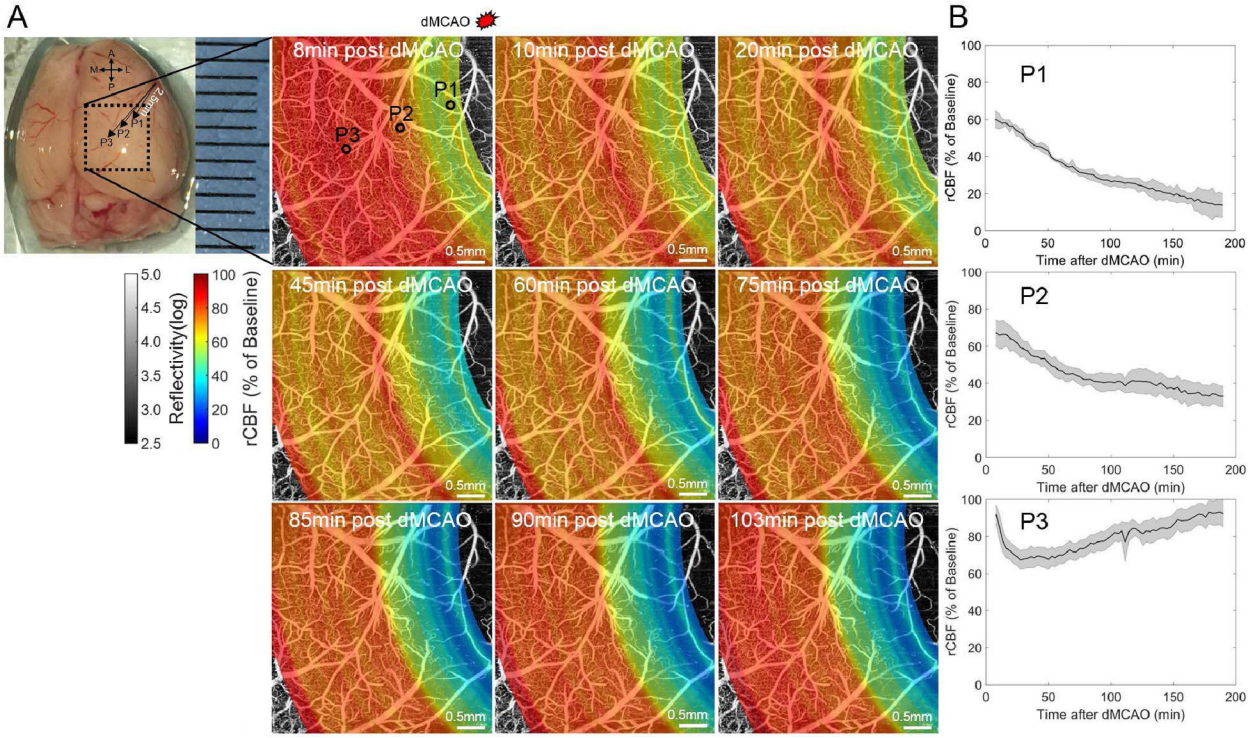

Fig. 4.

Spatiotemporal dynamics of the CBF responses to acute cerebral ischemia illustrate the relative change in CBF following transient dMCAO. (A) Time course of pseudo-colored relative CBF (rCBF) maps overlaid with the corresponding OMAG images (gray scale). The wanner color represents the higher percentage (%) of baseline CBF level. (B) Averaged traces of rCBF responses at three different positions; P1, P2, and P3 in the cranial window for all of 5 mice during ischemia, showing acute stroke-related relative changes in CBF against the baseline. The shaded region indicates two standard deviations around the averaged line. Each position (PI, P2, and P3) was 2.5 mm, 3.5 mm, and 4.5 mm distant away from the origin of occlusion. Top left insert in (A) is photograph of the harvested brain.

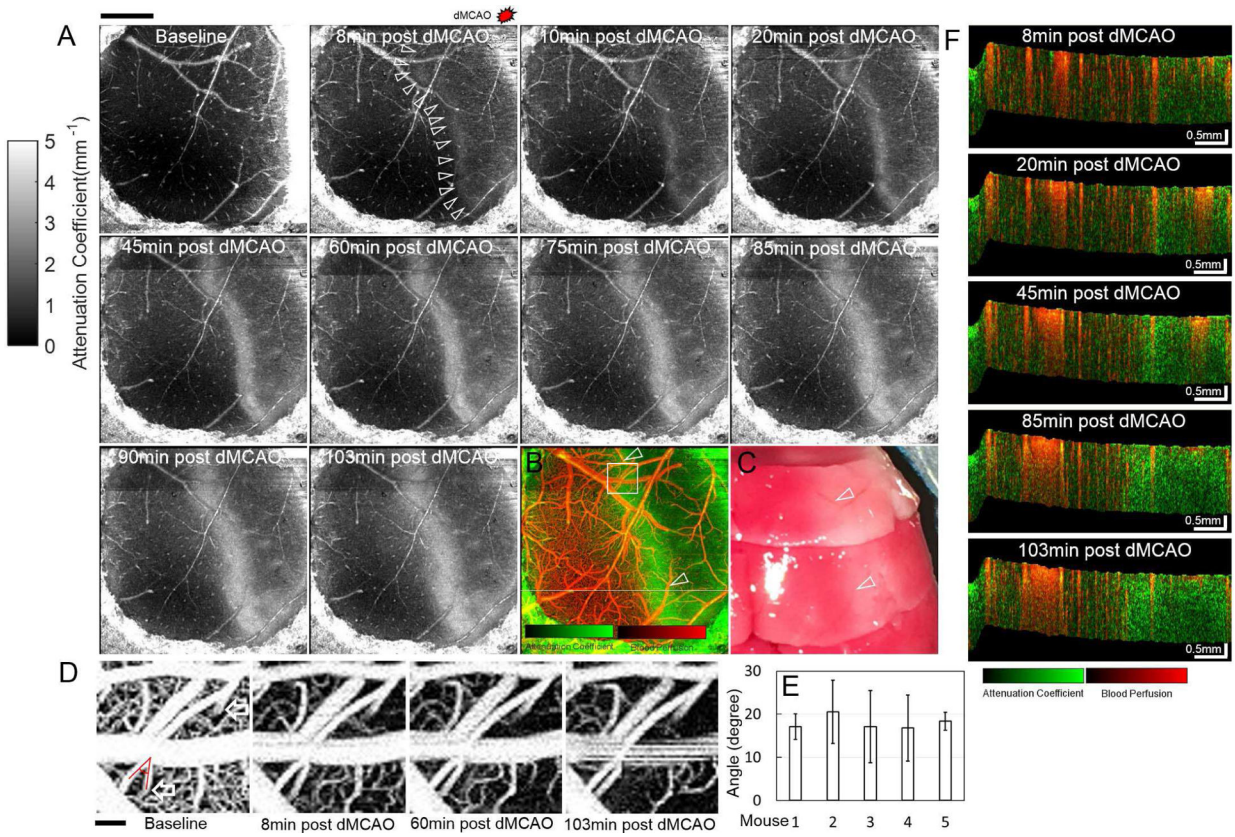

Fig. 5.

Changes in cortical tissue scattering from the attenuation coefficient measurements of the mouse brain during acute ischemic stroke. (A) Evolution of attenuation coefficients in the cerebral cortex after transient MCA occlusion. The cortical region proximal to the MCA (right lateral side of the cortex) has relatively high attenuation coefficients compared to the contralateral side and they are demarcated from a characteristic border zone lying along the cortex with much higher attenuation coefficients (arrow heads) that emerged 8 minutes after the dMCAO and diffusively enlarged in width over time. Scale bar is 1 mm. (B.) Overlay of OMAG image (red) and attenuation coefficient map (green) 130 minutes after dMCAO. (C) Top view of reassembled coronal brain sections with TTC staining 130 minutes after dMCAO. Infarct area appears as white and normal tissue appears as red. Arrow heads indicate vessel branches, similar to the pial arteries (arrow heads in (B)). (D) Change in location of the penetrating vessels (arrows) relative to the baseline in a small area (white box in (B)). Scale bar is 100/mi. The vascular displacement is measured as a change in angle between the penetrating vessel and its pial vessel. The measurement result (avg ± std) for each mouse is shown in (E). (F) Time course of blood perfusion (red) and attenuation (green) in the cross-sectional cortical tissue from the surface to 350 μm in depth taken at position (a white line in (B)).